Effects of Friction Stir Process Parameters on Microstructure and Mechanical Properties of Aluminum Powder Metallurgy Parts

Mohsen Abbasi-Baharanchi[1]*, Fathallah Karimzadeh[2], Mohammad Hossien Enayati[2]

[1] *Young Researchers and Elite Club, Najafabad Branch, Islamic Azad University, Najafabad, Iran;*
[2] *Department of Materials Engineering, Isfahan University of Technology, Isfahan, Iran*

ARTICLE INFO	ABSTRACT

The effects of friction stir processing (FSP) on the microstructure and mechanical properties of aluminum powder metallurgy (PM) parts were investigated. PM parts were subjected to FSP at advancing speeds (v) of 40-200 mm/min and tool rotational speeds (ω) of 800-1600 rpm. Microhardness (HV) and tensile tests at room temperature were used to evaluate the mechanical properties of the friction stir processed specimens. In order to evaluate microstructure of the processed zone, cross-sections of the FS processed specimens were observed optically. Based on the results obtained from investigation of the Zener-Holloman parameter (Z), the average grain size decreased with decreasing the working temperature and increasing the working strain rate (equal to increasing Z). The finest grain size was ~ 5.4µm obtained at ω=1000 and v =100 mm/min corresponding to a strain rate of $27s^{-1}$ at $414\,^\circ C$. This sample exhibited the best mechanical properties with microhardness, yield stress, and tensile strength of 43 Hv, 82 MPa, and 118.3 MPa, respectively.

1. Introduction

Mishra et al. developed friction stir processing (FSP) as a new solid state processing technique for microstructural modification based on friction stir welding (FSW)[1]. They reported friction stir welding creates bonds through the combined effects of heat, deformation by a stirring action, and pressure using a nonconsumable tool that is translated along a joint line. While it uses the same type of equipment and procedures, friction stir processing is not meant to bond materials together. Instead, friction stir processing is a means for locally modifying properties over depths or volumes that depend on the material being processed in order to produce the desired effect. For FSP, a location within a plate or sheet is selected into which a specially designed rotating tool is plunged. The tool has a larger diameter shoulder with a concentric small diameter pin. The rotating pin contacts the surface and heats it by friction as it descends into the part. When the shoulder contacts the work surface, its rotation causes additional frictional heat, thus plasticizing a larger cylindrical metal column around the inserted pin. The area to be processed and the tool are moved relative to each other such that the tool traverses the area until the entire selected area is processed to a fine grain size with the material transported from the leading to the trailing face of the pin. As the processed zone cools without solidification, it forms a defect-free recrystallized fine grain microstructure. FSP has many applications such as producing fine-grained microstructures and fabricating surface composites [2-6] . Aluminum alloys constitute a significant portion of lightweight metals used in industry. Certain

* Corresponding Author:
  E-mail Address: m.abbasi@ma.iut.ac.ir

properties of aluminum and its alloys such as low density, recyclability, ductility, and formability have made them especially suitable for a variety of industrial and automotive applications. Among them, aluminum powder metallurgy parts have attracted special attention. One of the attractions of powder metallurgy, as a fabrication approach, lies in its potential to fabricate precise, low-cost parts, which are applied in specific areas where the net-shaping capabilities can be combined with good properties. However, aluminum PM parts have limited applications because of their inadequate elastic modulus, wear resistance, or low mechanical properties. These shortcomings call for alternatives to conventional aluminum alloys. This paper aims to investigate the effects of friction stir processing parameters on the mechanical and microstructural properties of pure aluminum powder metallurgy parts.

2. Materials and methods

The starting material was aluminum powder (99.7% purity) which was cold compacted to $12 \times 20 \times 88 mm$ billets in a steel die set under a pressure of 225 MPa. To improve the billet strength for easier handling in FSP, the green compact was sintered for 20 min in air at 823 K. Sintered samples were subjected to FSP. Fig. 1 shows the geometry and dimensions of the FSP tool used here. The process conditions are described in Table 1. A schematic of the FSP setup is shown in Fig. 2. Upon processing, the specimens were cross-sectioned perpendicular to the process direction for metallographic analysis and mechanical tests. The cross-sections of the metallographic specimens were mechanically ground and polished by conventional methods and then etched in NaOH solution in water before being subjected to optical microscopy (OM) examination.

Fig 1. Illustration of the FSP tool used.

Table 1. FSP conditions.

$\omega\,(rpm)$	$v\,(mm\,/\min)$
800	40
	100
	160
	200
1000	40
	100
	160
	200
1250	40
	100
	160
	200
1600	40
	100
	160
	200

The Vickers hardness profiles of all the stir zones were measured on a cross-section perpendicular to the welding direction using a Vickers indenter under load of 5N for 15s. In order to evaluate the mechanical properties of specimens, tensile specimens with a gauge length of 26 mm and a width of 4 mm were cut from the SZ along the FSP direction and thinned to 2.5 mm thickness, with the top and bottom parts being removed by an electrical discharge machine. Tensile tests were carried out at room temperature at a crosshead speed of 2.5mm.min⁻¹, using a tensile testing machine. The mechanical

properties of the specimens were evaluated using three tensile specimens cut from the same original sample.

The temperatures along the interface during FSP were measured using K-type thermocouples (0.2 mm diameter) deployed at various locations from the process central line. The locations of the thermocouples are shown in Fig. 3.
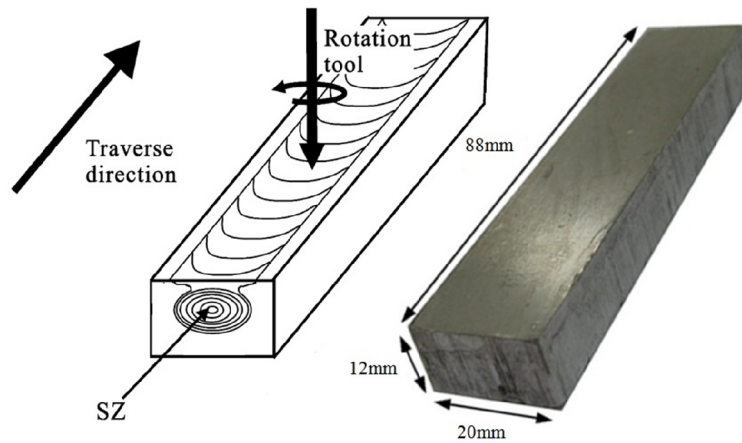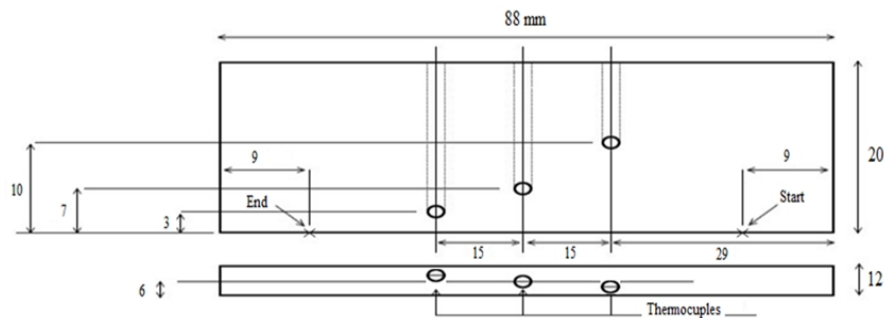

Fig 2. Schematic of the friction stir process [5].

Fig 3. Schematic of thermocouple locations within the specimens during FSP.

3. Results and discussion
A complete set of parameters presented in Table 1 were selected to identify the optimum FSP condition based on macroscopic, microscopic, and mechanical evaluations.

3.1. Macroscopic evaluation of stir zone
Fig. 4 depicts the appearance of the specimens after friction stir processing accomplished at rotational speeds of 800, 1000, 1250, and 1600 rpm and at traveling speeds of 40 and 200 mm/min (minimum and maximum traveling speeds, respectively). Clearly, increasing tool traveling speed (v) improved the appearance of the specimens while increasing tool rotational speed (ω) yielded more uniform sample surfaces. This is because of the increasing heat input during FSP resulting in increasing values of ω and v. Examination of specimen cross sections revealed certain defects in the form of post-FSP pores. Table 2 presents more details of the defects appearing after the process.
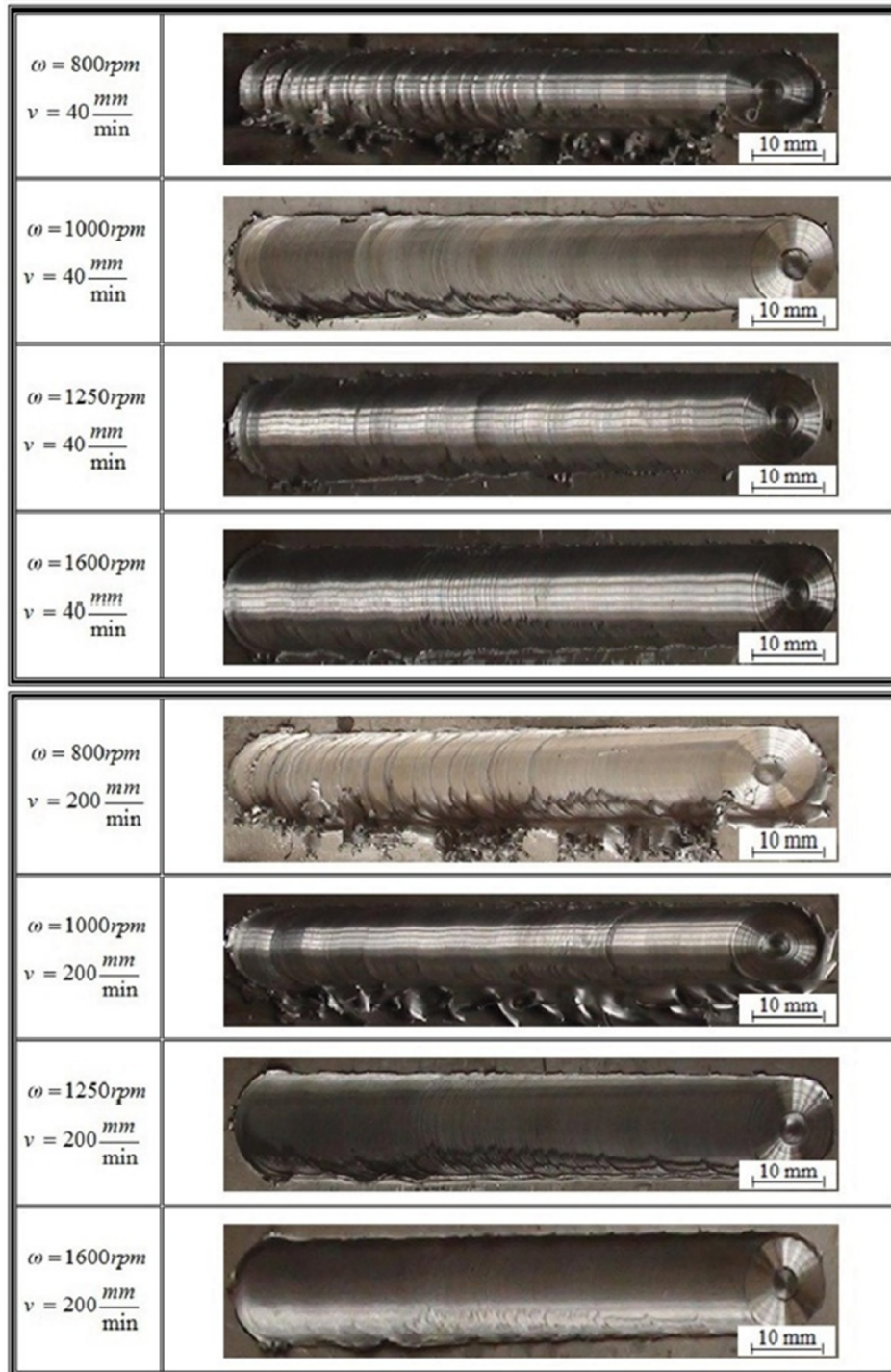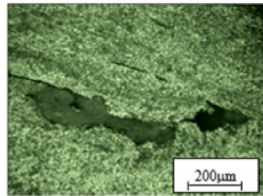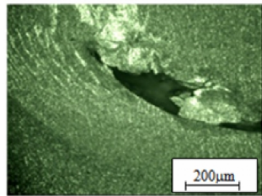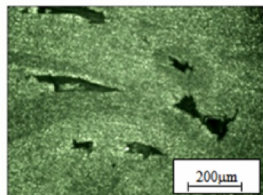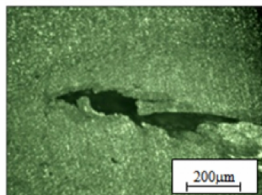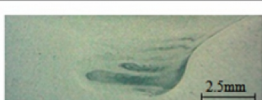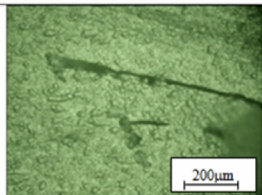
Fig 4. Specimens after FSP accomplished at different ω and ν speeds.

Table 2. Details of sound and defective specimens after FSP for different ω and v speeds.

Process Parameters	Cross Section	Process Parameters	Cross Section
$\omega = 800rpm$ $v = 40mm\,/\,min$ $\omega/v = 20$	2.5mm	$\omega = 800rpm$ $v = 100mm\,/\,min$ $\omega/v = 8$	2.5mm
$\omega = 800rpm$ $v = 160mm\,/\,min$ $\omega/v = 5$	200µm	$\omega = 800rpm$ $v = 200mm\,/\,min$ $\omega/v = 4$	200µm

Process Parameters	Cross Section	Process Parameters	Cross Section
$\omega = 1000rpm$ $v = 40mm\,/\,min$ $\omega/v = 25$	2.5mm	$\omega = 1000rpm$ $v = 100mm\,/\,min$ $\omega/v = 10$	2.5mm
$\omega = 1000rpm$ $v = 160mm\,/\,min$ $\omega/v = 6.25$	200µm	$\omega = 1000rpm$ $v = 200mm\,/\,min$ $\omega/v = 5$	200µm

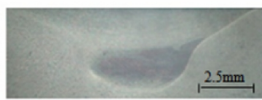| Process Parameters	Cross Section	Process Parameters	Cross Section
$\omega = 1250rpm$ $v = 40mm\,/\,min$ $\omega/v = 31.25$	2.5mm	$\omega = 1250rpm$ $v = 100mm\,/\,min$ $\omega/v = 12.5$	2.5mm
$\omega = 1250rpm$ $v = 160mm\,/\,min$ $\omega/v = 7.8$	2.5mm	$\omega = 1250rpm$ $v = 200mm\,/\,min$ $\omega/v = 6.25$	200µm

Process Parameters	Cross Section	Process Parameters	Cross Section
$\omega = 1600rpm$ $v = 40mm\,/\,min$ $\omega/v = 40$	2.5mm	$\omega = 1600rpm$ $v = 100mm\,/\,min$ $\omega/v = 16$	2.5mm
$\omega = 1600rpm$ $v = 160mm\,/\,min$ $\omega/v = 10$	2.5mm	$\omega = 1600rpm$ $v = 200mm\,/\,min$ $\omega/v = 8$	2.5mm

One of the most important technical parameters in FSP/W is the ω/v ratio [7]. In this research results have showed that the defects began to appear in specimens processed at

(ω/v)≤ 6.25. Hence further investigations of these samples were not considered. Frigaard et al. proposed the following equation for heat input during FSW [8]:

$$q = \frac{4}{3}\pi^2 \mu P \omega R^3 \qquad (1)$$

Where, q is heat input, μ is friction coefficient, P is pressure, ω is tool rotational speed, and R is shoulder radius. Based on equation 1, it is obvious that heat input depends on both the applied rotational speed and the shoulder radius. According to Frigaard et al. results, equation 2 expresses the heat input per unit length by taking tool travelling speed into account [8]:

$$Q = \frac{\alpha q}{v} = \frac{4}{3}\pi^2 \alpha\mu P \omega R^3 / v \qquad (2)$$

Where, α is a thermal coefficient and v is the tool travelling speed. In cases where α, μ, and R are fixed, Frigaard rewrote equation 2 as equation 3 [8]:

$$Q = P\frac{\omega}{v} \qquad (3)$$

It can be understood from Equation 3 that ω/v ratio is directly proportional to heat input so that decreasing the ratio will result in a corresponding decrease in heat input. In specimens FSPed at high tool traveling speeds (i.e., low ω/v ratios), the heat input is too low for the material to flow; hence, the grooves due to the pin travel over the specimen will not be completely filled and defects will, consequently, appear. Results indicate that defects appeared in samples which were processed at (ω/v)≤ 6.25. Therefore, process parameters that resulted in defected specimens were discarded in the remaining experiments.

3.2. Microscopic evaluation of the stir zone

The microstructure of the specimen processed at ω =1000 rpm and v =100 mm/min is shown in Fig. 5, depicting the stir zone, the thermomechanically affected zone, and the base metal. Fine, equiaxed grains form in the stir zone are as a result of dynamic recrystallization during thermomechanical deformation [9]. In Fig. 5, the TMAZ area located between the stir zone and the base metal consists of partially recrystallized gains.
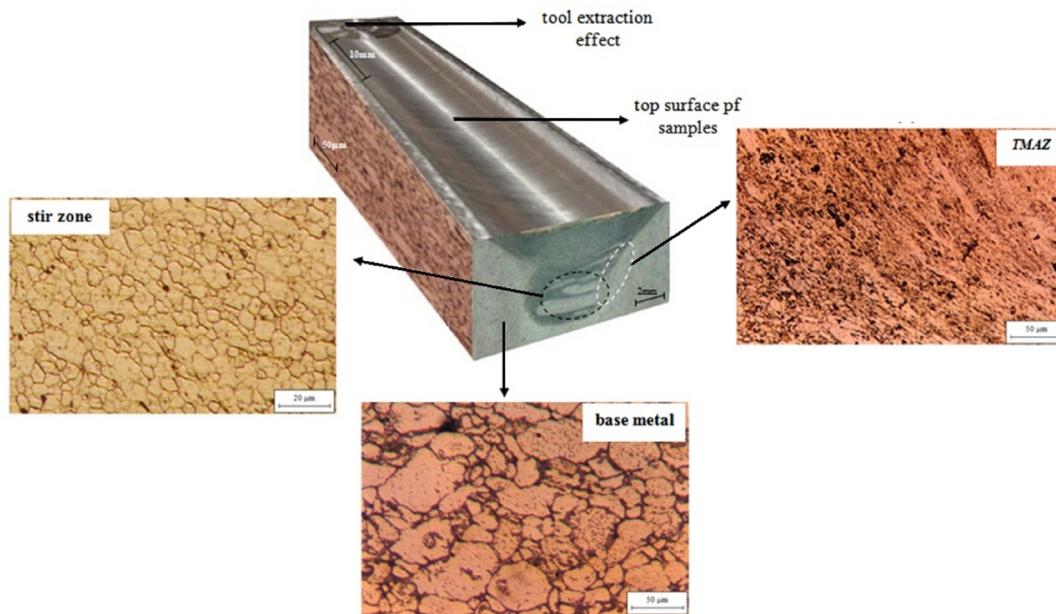
Fig 5. Different areas produced as a result of friction stir processing at ω =1000 rpm and v =100 mm/min.

Other features of the stir zone microstructure include onion rings as shown in Fig. 6. These rings appear due to the heat generated by the friction between the shoulder and the sample and also due to the extrusion of material caused by the travel of the tool [10].

It is clear from Fig. 6 that ring thickness increased toward the middle of the stir zone and

decreased around the edges of the surface. Ring spacing is directly proportional to the tool travelling speed but inversely related to the tool rotational speed.

Fig 6. Onion rings in the stir zone.

Theoretical considerations revealed that the distance between the grooves on sample surfaces is a function of the tool travel at the time it rotates around itself. For instance, the distance between the grooves on the surface of the specimen processed at ω =1000 rpm and v =100 mm/min was about 0.1mm. Fig. 7 shows these surface grooves for the specimen in question in which the groove distances are about 0.13mm, which is really close to its predicted value.

Microstructural investigations revealed that fine, equiaxed grains are formed in the stir zone. Variations of grain size in the stir zone after processing for different values of process parameters are presented in Fig.8.

Dynamic recrystallization is the most important mechanism involving grain refinement in the stir zone during FSP [9].
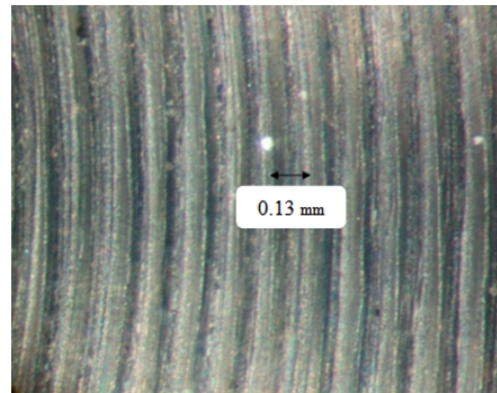
Fig 7. Surface grooves on the specimen processed at ω =1000 rpm and v =100 mm/min.
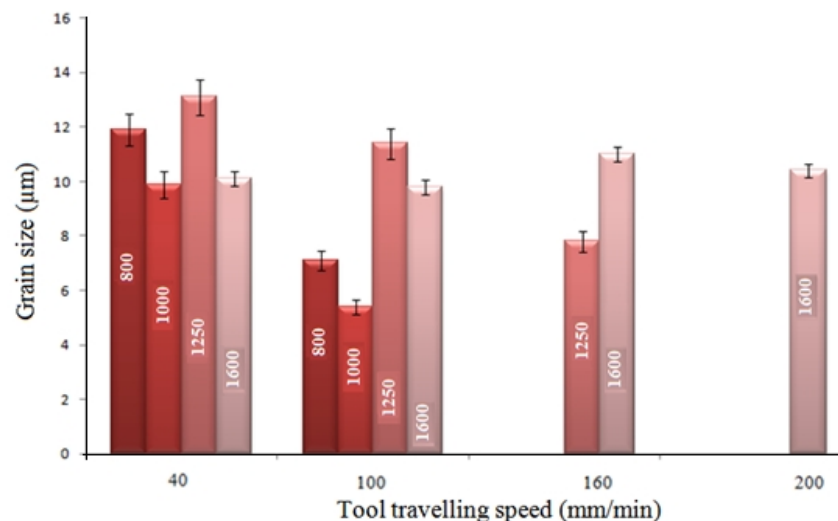
Fig 8. Variation in grain size in the stir zone after processing for different values of process parameters.

Based on the results it is found that increasing tool travelling speed resulted in reduced grain size. As already mentioned above, heat input decreases during friction stir processing with increasing tool traveling speed. At low tool travelling speeds there is less time available for grain growth, resulting in smaller grains formed in the stir zone [11]. Similarly, decreasing grain size with increasing welding speed may be the result of strains exerted to the material. High tool rotational speeds result in increasing temperature and decreasing cooling

rates, which ultimately lead to grain growth [12]. Investigation of the grain size in the specimens showed that the minimum grain size was 5.4 μm for sample processed at ω =1000 rpm and v =100 mm/min. It should be possible to investigate the effects of strain rate and temperature simultaneously (or, the Zener-Holloman parameter) on grain size in the stir zone as a result of variations in tool travelling and rotational speeds.

3.2.1. Strain rate in friction stir processing
Material flow during FSP was driven by the rotating pin. The flow rate may be compatible to or lower than the rotational speed of the pin [13]. Since there would usually be a certain level of rotation lagging effect by a linear assumption, the average material flow rate, R_m, is about half the pin rotational speed, R_p. Material flow strain rate, $\dot{\varepsilon}$, during FSP may be driven by the torsion-type deformation as follows [13]:

$$\dot{\varepsilon} = \frac{R_m 2\pi r_e}{L_e}$$

(4)

Where, r_e and L_e are the effective (or average) radius and depth of the dynamically recrystallized zone. All materials within the dynamically recrystallized zone would undergo the plastic flow and that such a zone typically appears as an onion in shape [10]. An effective radius, r_e, that can represent the average radius for all parts of the material inside this zone is assumed to be almost equal to 0.78 (or $\pi/4$) of the observed zone boundary radius, r_b [7]. A similar argument can be put forward for L. For a given Rp of 1000 rpm (or 16.6 rps, rotation per second) with r_b~2mm and L_b~3.3mm (Fig. 9), then $\dot{\varepsilon}$ is calculated to be ~27s^{-1}. For the currently applied rotational speeds varying from 800 to 1600 rpm, the typical strain rate will be scattered within 21-49^{-1}. Fig. 10 illustrates the effect of tool rotational speed on strain rate. It is clear from equation 4 that the higher the tool rotational speed, the higher will be the strain rate.
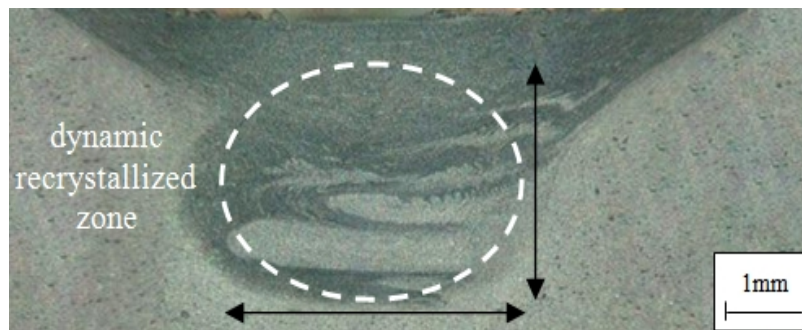

Fig 9. Cross section of the specimen processed at ω =1000 rpm and v =100 mm/min along with the dynamically recrystallized zone.
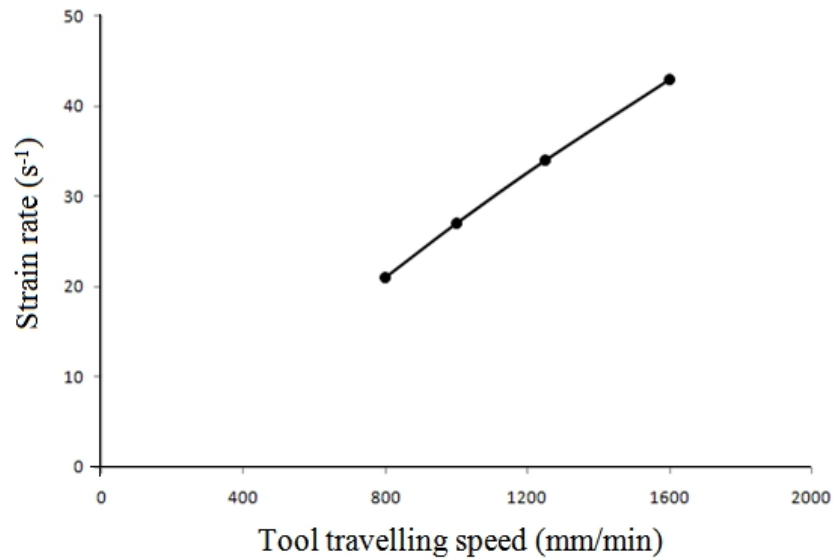
Fig 10. The effect of tool rotational speed on strain rate at a fixed tool traveling speed of v=100 mm/min.

3.2.2. Temperature distribution during friction stir processing

Fig. 11 presents temperature distribution during FSP at ω =1000 rpm and v =100 mm/min in three different areas including the one under the pin, that under the shoulder, and the area under the base metal. Arbegast and Hatherly investigated the effects of FSP parameters on temperature [14]. They reported that for a given tool geometry and depth of penetration, maximum temperature was observed to be a function of rotation rate. They observed that for several aluminum alloys, a general relationship between maximum welding temperature (T,ºC) and FSP parameters (ω and v) can be expressed by [14]:

$$\frac{T}{T_m} = k\left(\frac{\omega^2}{v \times 10^4}\right)^{\alpha}$$

(5)

Where, the exponent α was reported to range from 0.04 to 0.06, the constant, k, ranged between 0.65 and 0.75, and T_m(ºC) designated the melting point of the alloy.
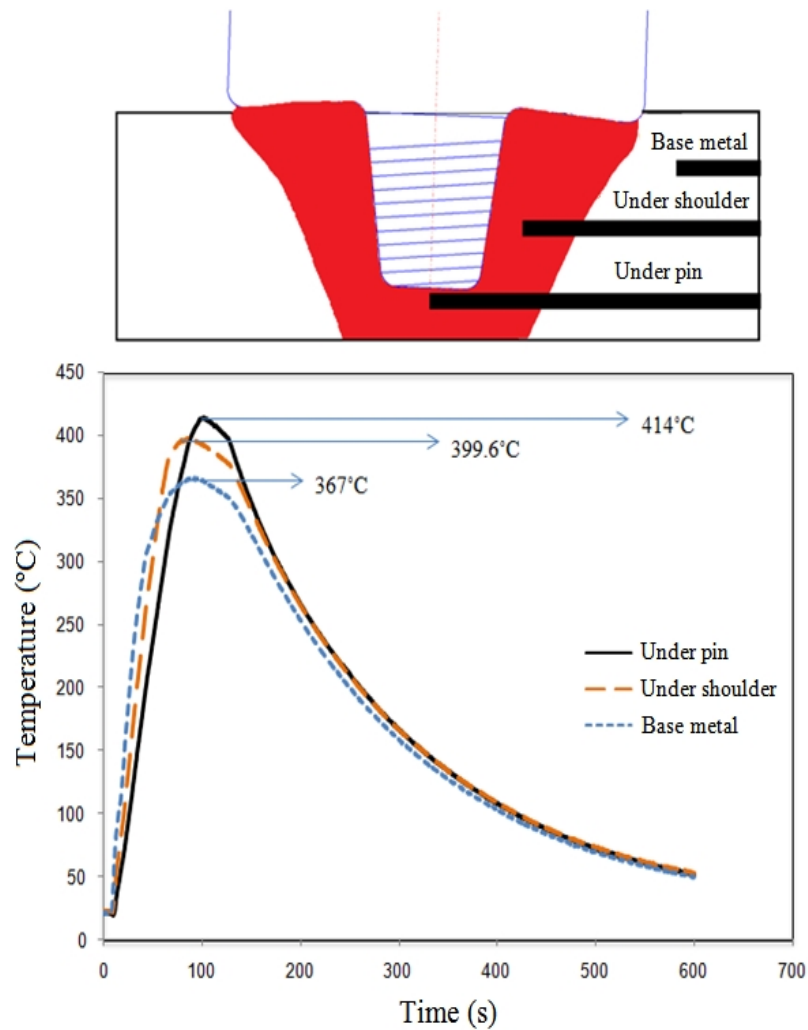
Fig 11. Temperature distribution in different areas during FSP at ω=1000 rpm and v=100 mm/min.

According to Fig. 12 and based on equation 5, the values for the exponent α and the constant k were found to be 0.043 and 0.632, respectively, during FSP of pure aluminum powder metallurgy parts. It is clear from equation 5 that tool rotational speed has a greater effect on stir zone temperature than tool traveling speed does.

Fig. 13 presents temperature variations in the stir zone with changing tool rotational and traveling speeds. Clearly, the higher the tool rotational speed, the higher the temperature.

Fig 12. Calculation of the exponent α and the constant k in Equation 5.
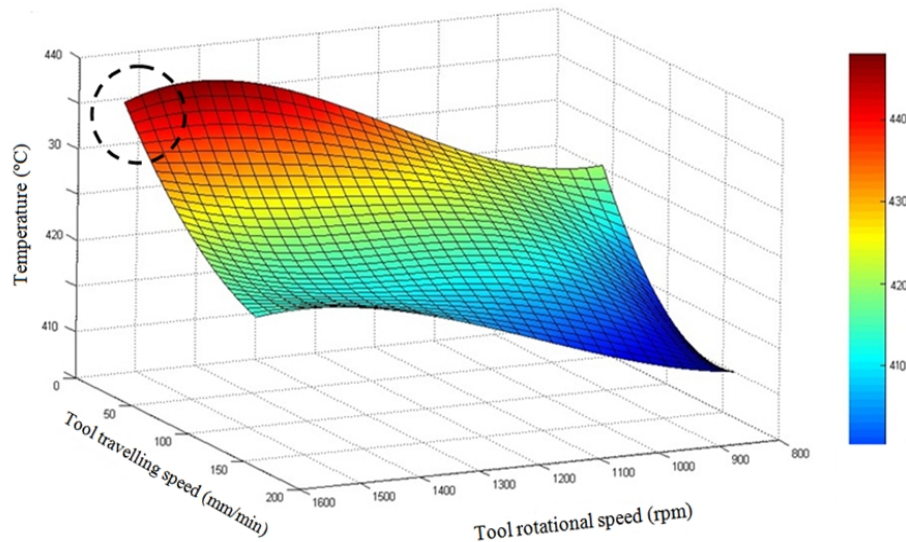
Fig 13. Variations in stir zone temperature with varying tool rotational and traveling speeds during FSP.

The increase in temperature is due to the friction between the tool and the specimen as well as the plastic deformation of the material [9]. On the other hand, it is observed tha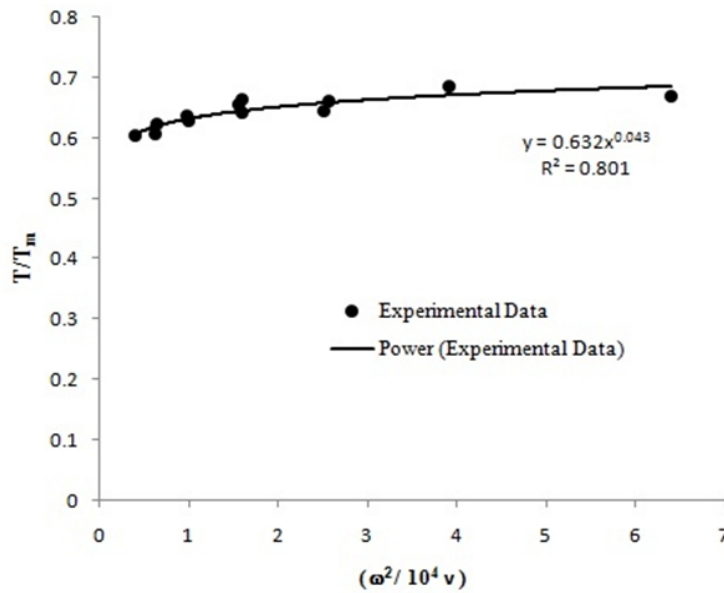t the higher the tool traveling speed, the lower is the temperature. In the friction stir process, tool traveling speed controls heat concentration, which means that heat concentration decreases with increasing tool traveling speed, thereby decreasing the maximum temperature [15]. It can be noticed in Fig. 13 that at high tool rotational speeds ($\omega \geq 1400$ rpm), temperature does not increase with increasing speed; thus, local melting affects temperature. Two reasons may be claimed to explain this phenomenon: 1) the coefficient of friction decreases when a local melt occurs following a local heat input; 2) the latent heat absorbs some of the heat input [12]. Fig. 14 shows temperature distribution across the specimens' width during FSP at $\omega =1000$ rpm and v=100 mm/min.

Fig 14. Temperature distribution across the specimens' width during FSP at ω=1000 rpm and v=100 mm/min.
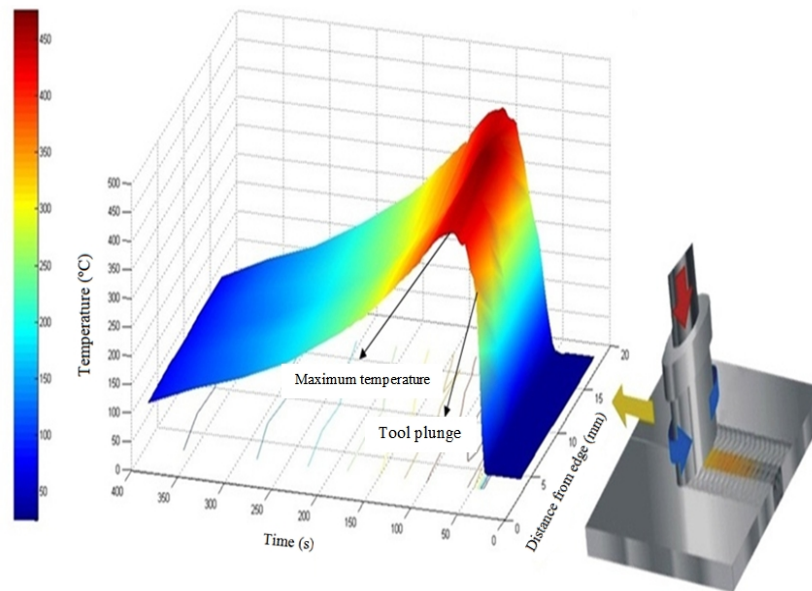
3.2.3. Effect of temperature and strain rate on recrystallized grain size

At temperatures where thermally activated deformation and restoration process occur, the microstructural evaluation will be dependent on deformation temperature (T) and strain rate ($\dot{\varepsilon}$), in addition to strain (ε). The strain rate and deformation temperature can be combined into a single parameter - the Zener-Holloman parameter (Z) - which is defined as [16]:

$$Z = \dot{\varepsilon}\exp(\frac{Q}{RT})$$

(6)

Where, Q is activation energy and R is gas constant. Table 3 presents the values for measured temperature, strain rate, Zener-Holloman parameter, and the corresponding grain size of specimens subjected to FS

processing at different ω and v speeds. For calculating the value of Zener-Holloman parameter, the value of activation energy (Q) was taken to be equal to158.3kg/mole for pure aluminum [16]. Relevant data are presented in Table 3 and Figs. 15 and 16. Clearly, grain size in the stir zone decreases with increasing values of Z. The highlighted zones in Figs. 15 and 16 correspond to (ω/v)≤6.25, resulting in defected specimens due to insufficient heat input. In general, the average grain size would decrease with decreasing working temperature and increasing working strain rate. In the present experiments, the finest grain size obtained was ~ 5.4µm for a rotational speed of 1000rpm corresponding to a strain rate of 27s^{-1} at a temperature of 414ºC.

Table 3. Measured temperature, strain rate, Z, and grain size in specimens processed at different values of ω and v.

$\omega(rpm)$	$v(mm/min)$	$T(\mathrm{°C})$	$\dot{\varepsilon}(s^{-1})$	$Z = \dot{\varepsilon}\exp\left(\dfrac{Q}{RT}\right)$	$D(\mu m)$
1600	40	436	43	1.97×10^{13}	10.1 ± 0.5
1600	100	437	43	1.90×10^{13}	9.8 ± 0.2
1600	160	438	43	1.83×10^{13}	11.0 ± 0.65
1600	200	433	43	1.75×10^{13}	10.4 ± 0.4
1250	40	437	34	1.50×10^{13}	13.1 ± 0.65
1250	100	432	34	1.82×10^{13}	11.4 ± 0.3
1250	160	427	34	2.21×10^{13}	7.8 ± 0.35
1000	40	425	27	1.89×10^{13}	9.9 ± 0.4
1000	100	414	27	2.94×10^{13}	5.4 ± 0.45
800	40	424	21	1.54×10^{13}	11.9 ± 0.3
800	100	412	21	2.47×10^{13}	7.1 ± 0.3

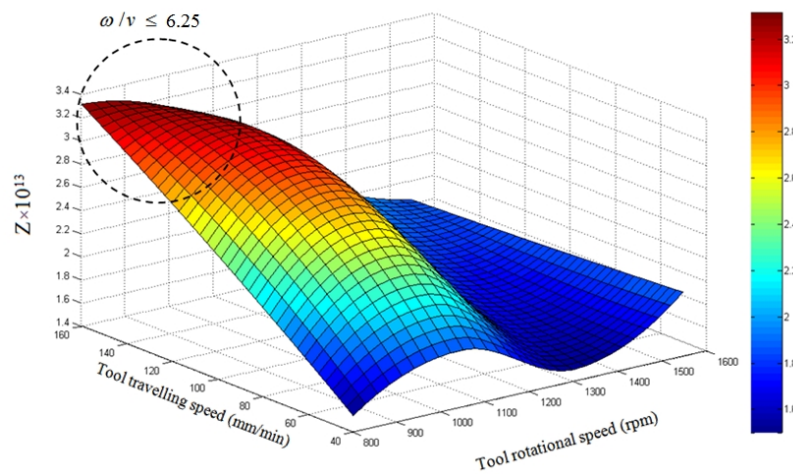**Fig 15.** Variations in Z as a function of ω and v.
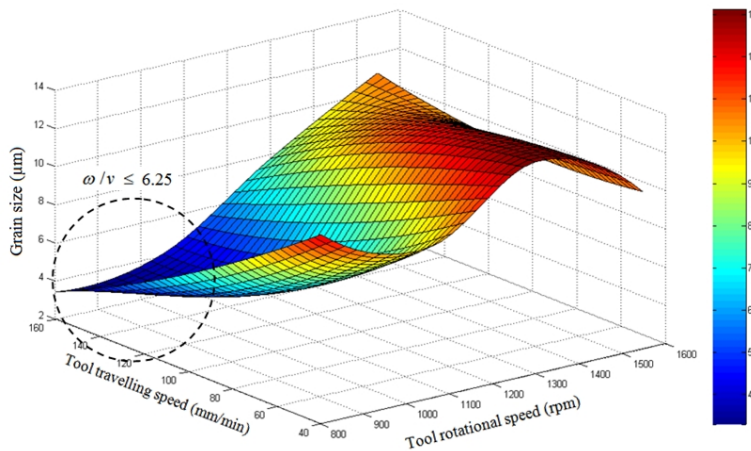

Fig 16. Variations in grain size with varying values of ω and v.

Rhodes et al. used the plunge and extract method of the rotating pin in 7050 Al alloys [17]. They demonstrated that the fine grains in such FSP specimens are identical to the recrystallized grains in specimens annealed at 350-450ºC for 1-4 min. Typical recrystallization

temperatures are around 0.6-0.8 T_m for Al alloys. The same range was obtained in the present study.

The relationship between the Zener-Holloman parameter and the average recrystallized grain size (D in μm) for pure aluminum during FSP is established in Fig. 17 and is given quantitatively by:

$$Ln(D) = 41.8 - 1.282 Ln(Z) \qquad (7)$$

In should be noted that the ranges for *D* and *Z* in the current FSP study are still rather narrow; the uncertainty is, thus, high.
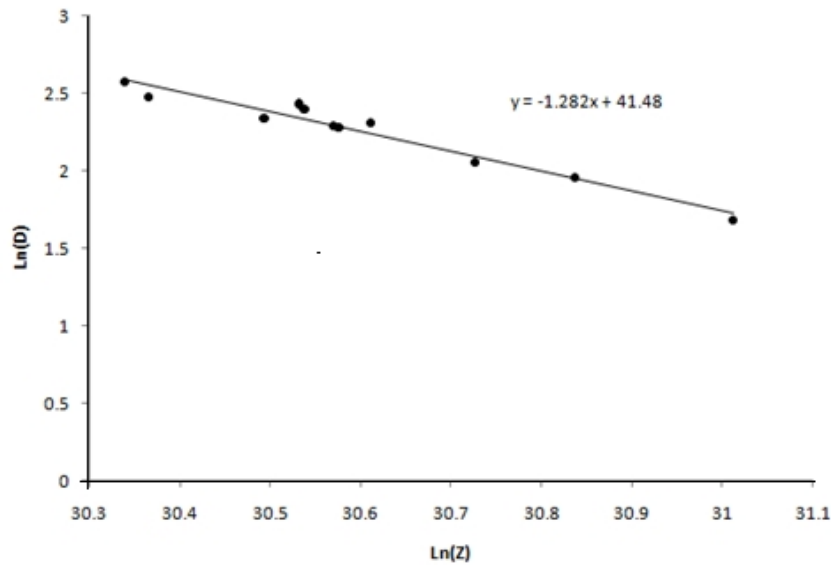

Fig 17. The relationship between Z and grain size in FSP.

The proposed mechanism for grain refinement in aluminum and aluminum alloys during FSP/W consists of dynamic recovery (DRV), geometric dynamic recrystallization (GDRX), and discontinuous dynamic recrystallization (DRRX). Dynamic recovery (DRV) takes place promptly during hot working of metals of high stacking fault energy such as aluminum [16]. The flow stress ascends during the initial period of deformation as dislocations increase and interact. However, the rate of recovery also increases as the dislocation density increases and dislocations begin to reorganize and form low-angle boundaries as subgrains develop. Finally, the flow stress saturates as hardening due to dislocation multiplication and recovery due to dislocation rearrangement reach a dynamic equilibrium. This leads to deformation at a steady-state wherein the flow stress remains constant with strain. The steady state is reflected in equiaxed subgrains with nearly dislocation-free interiors, constant subgrain size, and subgrain boundary

misorientation. The steady state appears to reflect continual processes of subgrain boundary formation, rearrangement and dissolution during deformation. During DRV, the flow stress, dislocation structure and texture evolution depend on the Zener–Hollomon parameter. Thus, flow stress and dislocation density increase while subgrain size decreases when Z increases. DRV reflects ease of climb and cross-slip in materials of high stacking fault energy; the corresponding deformation microstructures tend to be homogeneous, and the absence of local strain concentrations apparently precludes alternative restoration mechanisms.

The onset of geometric dynamic recrystallization (GDRX) may be observed as strain increases during DRV when the separation of prior boundaries approaches the subgrain size [9, 14]. During hot or warm rolling prior boundaries become serrated as they respond locally to the interface tensions of subgrain boundaries and develop waviness over distances on the order of the subgrain size. Then,

GDRX may occur when the prior boundary separation becomes equal to the subgrain size, which, in turn, is related to Z^{-1}. Thus, at low strain rates and stresses, the small values of Z will lead to the onset of GDRX at small strains, while at high strain rates and stresses the DRV stage of deformation will be more prolonged prior to the onset of GDRX. However, the recrystallized grain size will be finer when deformation takes place at higher values of Z.

The two former mechanisms are consistent with the current understanding of recrystallization in aluminum in light of its high stacking fault energy. However, DDRX, which has been cited in studies of FSP of AA7075, is inconsistent with the high stacking fault energy of aluminum [5]. Nevertheless, ultrafine grains have been observed in TEM investigations of this alloy for selected processing conditions.

3.3. Evaluation of mechanical properties

Fig. 18 presents the variation of stir zone microhandness for FS processed specimens with different values of ω and v. As it can be seen in Figure 18 and 19 microhardness and ultimate strength increase with increasing traveling speed at constant rotational rate. According to equation 5 at higher traveling speed shorter time is available for grain growth. The decrease in grain size with increasing traveling speed can also be attributed to greater straining of the metal which in turn motivates more strain-free nucleation sites [18]. The greater the nucleation rate, the more competitive the grain growth and therefore the finer the final grain size will be. As a result, improved mechanical properties are obtained.
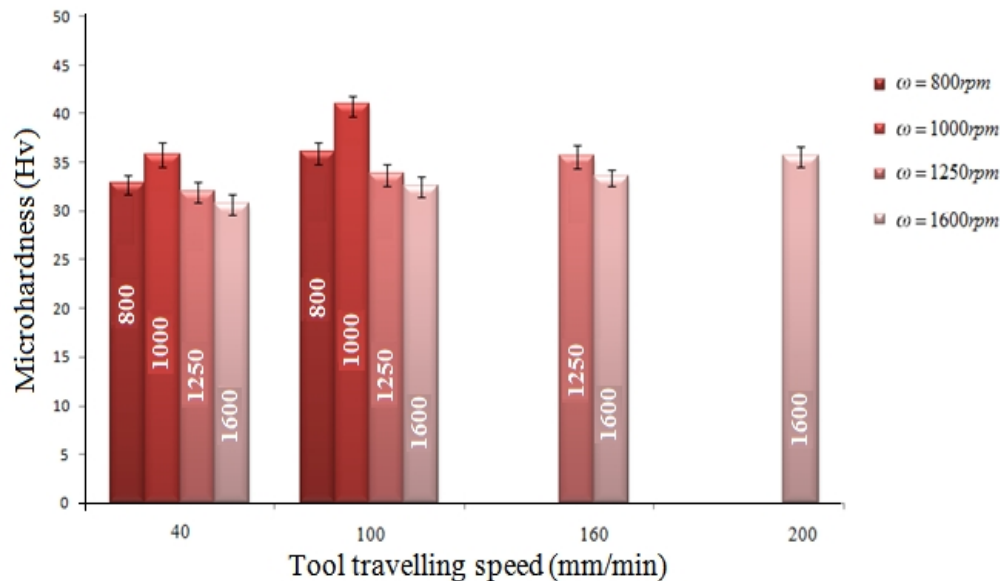

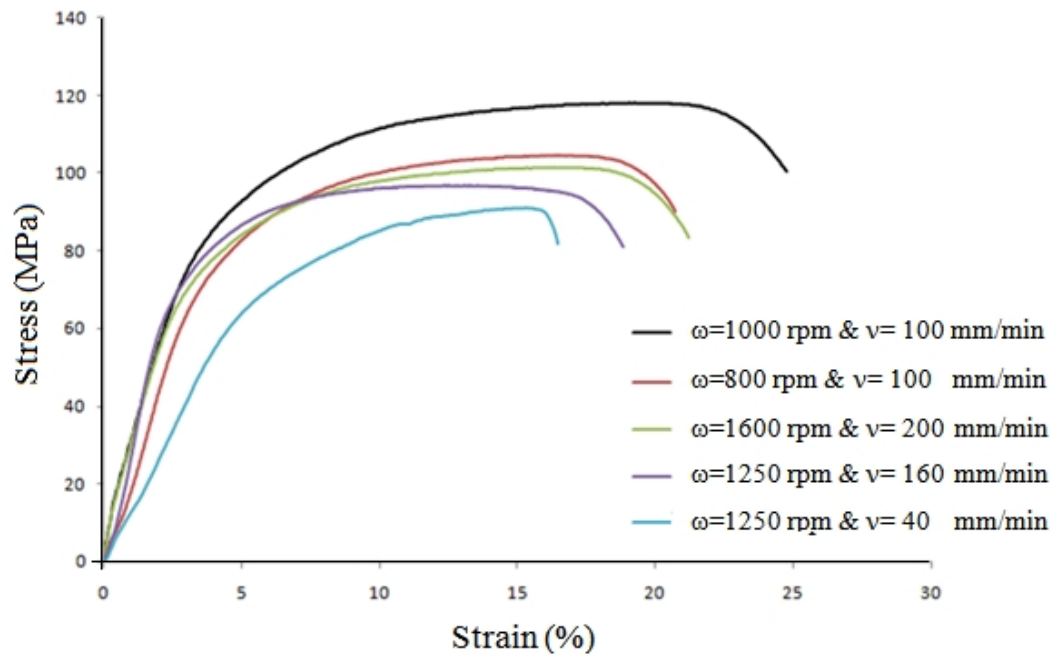**Fig 18.** Variations of microhardness in FS processed specimens.

Fig 19. Stress/strain tests for specimens processed at different ω and v speeds.

On the other hand, tool rotational speed has two distinct effects. According to equation 5, the more the tool traveling speed, the more the temperature is, which results in grain growth and decreasing mechanical properties. Additionally, based on equation 4, increasing tool rotational speed results in increasing strain rate and hence dislocations density increases and mechanical properties improve. So in general, the optimum mechanical properties are determined by considering simultaneous effects of tool travelling and rotational speeds. Based on Figure 18, the maximum microhardness in the stir zone is related to the specimen processed at ω =1000 rpm and v =100 mm/min. The stress/strain records of the FS processed specimens are presented in Fig. 19 whereas Table 4 presents the tensile properties of the

friction stir processed specimens. The relationship between hardness, H_v, and the grain size in the stir zone have been examined using the hall-petch equation [19, 20]:

$$H_v = H_0 + k_h d^{-1/2} \tag{8}$$

Where, H_0 and k_h are the relevant constants. Because H_v is proportional to $d^{-1/2}$, the finer the grain size is, the higher will be the hardness value. As previously mentioned, the finest gain size was found to be related to maximum value of Z. Applying the same approach, it can be concluded that the improved tensile properties in the sample processed at ω =1000 rpm and v =100 mm/min are related to the fine grain structure produced as a results of recrystallization in the stir zone during FSP.

Table 4. Material properties of FS processed specimens, data acquired from tensile tests.

ω(rpm)	V(mm/min)	Yield stress (MPa)	UTS (MPa)	Elongation (%)
1000	100	82±3.2	118.3±4.3	18.4±2.0
800	100	73±4.7	104.7±4.1	14.2±2.5
1600	200	69±4.1	103.4±3.3	15.8±2.0
1250	160	65±3.9	98±4.0	13.1±2.4
1250	40	57±5.1	91.7±3.5	10.2±2.7

4. Conclusions

In this study, attempts were made to investigate the effects of friction stir processing parameters on the mechanical and microstructural properties of aluminum powder metallurgy parts. From this investigation, the following conclusions are derived:

(1) Among the process parameters including tool rotational speeds from 800 to 1600rpm and tool travelling speed from 40 to 200mm/min, defected specimens were found for $(\omega/v) \leq 6.25$.

(2) Increasing tool travelling speed leads to decreasing heat input, resulting in decreased grain size.

(3) In light of the Zener-Holloman parameter, average grain size decreases with decreasing working temperature and increasing working strain rate (equals to increasing Z). The finest grain size obtained in the present experiments was equal to ~ 5.4μm for a tool rotational speed of 1000rpm and a tool travelling speed of 100 mm/min corresponding to a strain rate of $27s^{-1}$ at of 414 ºC.

(4) The best mechanical properties were observed in the specimen processed at ω =1000 rpm and v=100 mm/min corresponding to the minimum grain size. The values of microhardness, yield stress, and tensile strength of the tested specimens were found to be 43 Hv, 82 MPa, and 118.3 MPa, respectively.

References

[1] R. S. Mishra, M. W. Mahoney, S. X. McFadden, N. A. Mara, and A. K. Mukherjee, "High strain rate superplasticity in a friction stir processed 7075 Al alloy," Scripta Mater. J., vol. 42, 2000, pp. 163–168.

[2] W. B. Lee, Y. M. Yeon, and S. B. Jung, "The improvement of mechanical properties of friction-stir-welded A356 Al alloy," Mater. Sci. Eng. A J., vol. 355, 2003, pp. 154–159.

[3] Z. Y. Ma, R. S. Mishra, and M. W. Mahoney, "Superplasticity in cast A356 induced via friction stir processing," Scripta Mater. J., vol. 50, 2004, pp. 931–935.

[4] R. S. Mishra, Z. Y. Ma, and I. Charit, "Friction stir processing: A novel technique for fabrication of surface composite," Mater. Sci. Eng. A J., vol. 341, 2003, pp. 307–310.

[5] C. J. Hsu, P. W. Kao, and N. J. Ho, "Ultrafine-grained Al-Al2Cu composite produced in situ by friction stir processing," Scripta Mater. J., vol. 53, 2005, pp. 341–345.

[6] A. S. Golezani, M. Esmaily, and N. Mortazavi, "A study on the sub-structure and mechanical properties of friction stir processed AA 6061-T6 joints with ultra-fine grained structure," Adv. Mater. Process. J., vol. 2, 2014, pp. 33–46.

[7] M. Abbasi Gharacheh, A. H. Kokabi, G. H. Daneshi, B. Shalchi, and R. Sarrafi, "The influence of the ratio of 'rotational speed/traverse speed' (ω/v) on mechanical properties of AZ31 friction stir welds," Mach. Tool. Manu. J., vol. 46, 2006, pp. 1983–1987.

[8] Ø. Frigaard, Ø. Grong, and O. T. Midling, "A process model for friction stir welding of age hardening aluminum alloys," Metall. Mater. Trans. A J., vol. 32, 2001, pp. 1189–1200.

[9] T. R. McNelley, S. Swaminathan, and J. Q. Su, "Recrystallization mechanisms during friction stir welding/processing of aluminum alloys," Scripta Mater. J., vol. 58, 2008, pp. 349–354.

[10] K. N. Krishnan, "On the formation of onion rings in friction stir welds," Mater. Sci. Eng. A J., vol. 327, 2002, pp. 246–251.

[11] X. Cao and M. Jahazi, "Effect of welding speed on the quality of friction stir welded butt joints of a magnesium alloy," Mater. Design J., vol. 30, 2009, pp. 2033–2042.

[12] K. Elangovan and V. Balasubramanian, "Influences of pin profile and rotational speed of the tool on the formation of friction stir processing zone in AA2219 aluminium alloy," Mater. Sci. Eng. A J., vol. 459, 2007, pp. 7–18.

[13] C. I. Chang, C. J. Lee, and J. C. Huang, "Relationship between grain size and Zener–Holloman parameter during friction stir processing in AZ31 Mg alloys," Scripta Materi. J., vol. 51, 2004, pp. 509–514.

[14] W. J. Arbegast and P. J. Hartley, "Friction Stir Weld Technology Development at Lockheed Martin Michoud Space System - An Overview," in *TRENDS IN WELDING RESEARCH -INTERNATIONAL CONFERENCE*, 1998, pp. 541–546.

[15] K. Elangovan and V. Balasubramanian, "Influences of tool pin profile and welding

speed on the formation of friction stir processing zone in AA2219 aluminium alloy," Mater. Proc. Tech. J., vol. 200, 2008, pp. 163–175.

[16] F. J. Humphreys and M. Hatherly, Recrystallization and related annealing phenomena, 2ed. University of Manchester Institute of Science and Technology, Oxford, 2004, p.417.

[17] C. Rhodes, "Fine-grain evolution in friction-stir processed 7050 aluminum," Scripta Mater. J., vol. 48, 2003, pp. 1451–1455.

[18] M. Pareek, A. Polar, F. Rumiche, and J. E. Indacochea, "Metallurgical evaluation of AZ31B-H24 magnesium alloy friction stir welds," Mater. Eng. Performance J., vol. 16, 2007, pp. 655–662.

[19] Y. S. Sato, M. Urata, H. Kokawa, and K. Ikeda, "Hall-Petch relationship in friction stir welds of equal channel angular-pressed aluminium alloys," Mater. Sci. Eng. A J., vol. 354, 2003, pp. 298–305.

[20] T. Hirata, T. Oguri, H. Hagino, T. Tanaka, S. W. Chung, Y. Takigawa, and K. Higashi, "Influence of friction stir welding parameters on grain size and formability in 5083 aluminum alloy," Mater. Sci. Eng. A J., vol. 456, 2007, pp. 344–349, 2007.